網膜症も１１例全例[3]で遺伝子の異常が検出され、これらの疾患は単一遺伝子疾患であることを確認した。これらの疾患では遺伝子変異が確認された症例の臨床像をかえりみることによって、病気の phenotype の特徴を再確認できた。

一方、原因となる疾患が異なるにもかかわらず、それぞれの疾患としては特殊な臨床像を呈するために、類似した臨床像を示す場合があった。たとえば黄斑変性と negative type の ERG を合併した臨床像を呈する場合、これはひとつの疾患単位なのではなく、この中には黄斑の網膜分離が黄斑変性となった若年網膜分離症や[4]、ERG の反応が非典型的なスタルガルト病、ERG が negative type を示す錐体杆体ジストロフィの場合が含まれていた。

また視神経萎縮と negative type の ERG を合併しているという症例には、通常は合併しない視神経萎縮を合併している不全型先天停止性夜盲や[5]、通常とは異なり ERG が negative type を示す常染色体優性視神経萎縮[6]が含まれていた。これらの症例では遺伝子検査によってはじめて診断可能だった。

D．考察

最近は近親婚の減少や少子化の影響で家族歴のない場合が増えており、今後も孤発例は増加すると考えられる。

遺伝子診断を行うことによって、疾患の phenotype の特徴を再確認できた結果、遺伝子検査をしなくても、より確実な診断ができるようになった。

今回採血した 452 家系中、臨床像が非典型的なために、phenotype 分析だけでは診断することができない分類不能の症例が約 100 家系あった。その中には、遺伝子診断により始めて原因がわかる場合があった。網膜色素変性症や錐体杆体変性症といった多数の遺伝子が原因となる疾患では、未だに原因が同定できない場合が多いので、今後はその原因を突き詰めていくと共に、分類不能な非典型例の診断も、疾患の臨床像を理解するために行っていかなくてはならない問題と考えられる。

E．結論

計 452 家系 685 症例の遺伝性眼疾患の症例の原因遺伝子を検索し、155 家系で原因遺伝子を同定した。単一遺伝子疾患では、ほとんどの症例で遺伝子診断可能だった。表現型が非典型的な症例では、遺伝子診断によってのみ、診断可能な場合があった。網膜色素変性症や錐体（杆体）ジストロフィ等多くの遺伝子が原因となる場合や、臨床所見から診断不可能な症例では、原因遺伝子が同定できる場合はまだ多くない。

F．健康危険情報

なし

G．研究発表

１．論文発表

1. Nakamura M, Hotta Y, Tanikawa A, Terasaki H, Miyake Y: A high association with cone dystrophy in fundus albipunctatus caused by mutations of the RDH5 gene. Invest OphthalmolVisSci. 41: 3925-3932, 2000.
2. Nakamura M, Ito S, Terasaki H,

Miyake Y: Novel CACNA1F mutations in Japanese patients with incomplete congenital stationary night blindness. Invest Ophthalmol Vis Sci. 42: 1610-1616, 2001.
3. Lin J, Nishiguchi KM, Nakamura M, Dryja TP, Berson EL, Miyake Y: Recessive mutations in the CYP4V2 gene in East Asian and Middle Eastern patients with Bietti crytalline corneoretinal dystrophy. J Med Genet 42: e38, 2005.
4. Nakamura M, Ito S, Terasaki H, Miyake Y: Japanese X-linked juvenile retinoschisis: Conflict of phenotype:genotype with novel mutations in the XLRS1 gene. Arch Ophthalmol. 119: 1553-1554, 2001.
5. Nakamura M, Ito S, Piao CH, Terasaki H, Miyake Y: Retinal and optic disc atrophy associated with a CACNA1F mutation in a Japanese family.ArchOphthalmol. 121: 1028-1033, 2003.
6. Makoto Nakamura, Yozo Miyake: Optic Atrophy and Negative Electroretinogram in a Patient Associated with a Novel OPA1 Mutation. Graefes Archive for Clinical and Experimental Ophthalmology Jul 15: 1-2, 2005. [Epub ahead of print]

2．学会発表

なし

H．知的財産権の出願・登録状況

1．特許取得

なし

2．実用新案登録

なし

3．その他

なし

I．参考文献

なし

7. FSCN2 遺伝子変異マウスの開発とその網膜の解析

横倉俊二[1)]、和田裕子[1)]、佐藤　肇[1)]、中井茂康[2)]、
八尾良司[2)]、野田哲生[2)]、西田幸二[1)]
([1)] 東北大、[2)] (財) 癌研究会癌研究所)

研究要旨　我々は今回、FSCN2 遺伝子変異による網膜症の発症メカニズムを探るため、ヒトと同じ位置の１塩基を欠損させたマウス(p 型)と FSCN2 のエクソン１の大部分を破壊したマウス(g 型)をジーン・ターゲティング法を用いて作製し、それらの網膜の形態・機能を解析した。

$FSCN2^{p/p}$ マウスの網膜から抽出した mRNA は nonsense-mediate decay を呈した。$FSCN2^{+/p}$ マウスと $FSCN2^{+/g}$ マウスは光顕での観察で、加齢と共に進行する視細胞の変性を呈した。透過型電子顕微鏡での観察では、$FSCN2^{p/p}$ マウスと $FSCN2^{g/g}$ マウスの両方で異常な形態の外節が認められた。$FSCN2^{+/p}$ マウスと $FSCN2^{+/g}$ マウスの網膜電図を測定したところ、最初に杆体の機能が低下し、約 8 週程遅れて錐体の機能も低下することが明らかになった。これらの結果から、FSCN2 遺伝子異常では、FSCN2 遺伝子産物の haplo-insufficiency により外節板の形成が阻害され、ヒトの常染色体優性網膜色素変性症に類似した視細胞変性が引き起こされると考えられた。

A．研究目的

ヒト FSCN2 遺伝子は 17 番染色体長腕(17q25)に存在し、516 個のアミノ酸をコードしている。FSCN2 遺伝子は視細胞に特異的に発現しており、その遺伝子産物はアクチン結合・束状化活性を有している [1)]。本遺伝子変異患者は全て 208delG 変異を有しており、常染色体優性網膜色素変性症または常染色体優性黄斑変性症を発症する [2, 3)]。我々は今回、本遺伝子変異による網膜症の発症メカニズムを探るため、ヒトと同じ位置の１塩基を欠損させたマウス(p 型)と FSCN2 のエクソン１の大部分を破壊したマウス(g 型)をジーン・ターゲティング法を用いて作製し、それらの網膜の形態・機能を解析した。

B．研究方法

拙著 [4)] に示した通り、いわゆるジーン・ターゲティング法を用いて前出の２種類のマウスを作製した。遺伝子の発現については、生後８週の各遺伝子型マウス網膜 mRNA を用いた RT-PCR 法、及び同週齢マウスの網膜切片を用いた in situ hybridization 法にて解析した。形態学的な変化については、生後４、８、１６、２４週の各遺伝子型マウス網膜切片を作製し、H-E 染色による光顕的解析、及び電子顕微鏡的解析を行った。機能的な変化については、生後４、８、１６、２４、３２週の各遺伝子型マウスを用いた、暗順応及び明順応網膜電図にて解析した。尚、実験動物の取扱いに関しては、ARVO Statement for the Use of Animals in

Ophthalmic and Vision Research. に準拠して行った。

C. 研究結果

RT-PCR を施行した所、FSCN2$^{g/g}$ neo(-)のみならず、poly(A)シグナルの無い FSCN2$^{p/p}$ neo(-)マウスにおいても、mRNA がほぼ消失しており、nonsense-mediate decay の関与が示唆された(図 1)。in situ hybridization においても、FSCN2$^{p/p}$ neo(-)マウスで mRNA の消失が確認された [4]。

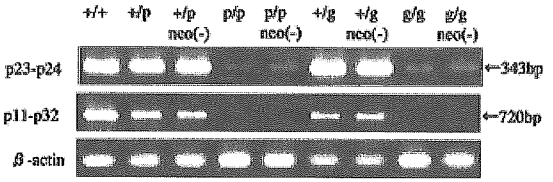

図 1　RT-PCR の結果

FSCN2$^{+/p}$ neo(-)の外節は野生型のそれよりも短かく(P<0.05)、外顆粒層は野生型よりも薄かった(P<0.05) (図 2A, B)。同じ週齢の FSCN2$^{p/p}$ neo(-)マウスは外節が FSCN2$^{+/p}$ neo(-)よりも更に短かかった (図 2C)。加齢によりこれらの変化は FSCN2$^{p/p}$ neo(-)マウスにおいても徐々に 進行することが判明した(図 2D-F)。これらのパラメータにつき、g 型のマウスも解析した所、p 型とほぼ同様の所見であった(図 2G-J)。

次に各マウスの視細胞の超微形態を、透過型電子顕微鏡を用いて解析したところ、生後 4 週では、FSCN2$^{+/p}$ neo(-)マウスの外節は野生型のそれより短いものの、ほぼ同様の形態であった [4]。しかし FSCN2$^{p/p}$ neo(-)マウスの外節は異常な屈曲を呈していた [4]。これらの変化は加齢と共に増強された [4]。同様に g 型についても外節の超微形態を観察したが、やはり p 型と同様の所見であった [4]。

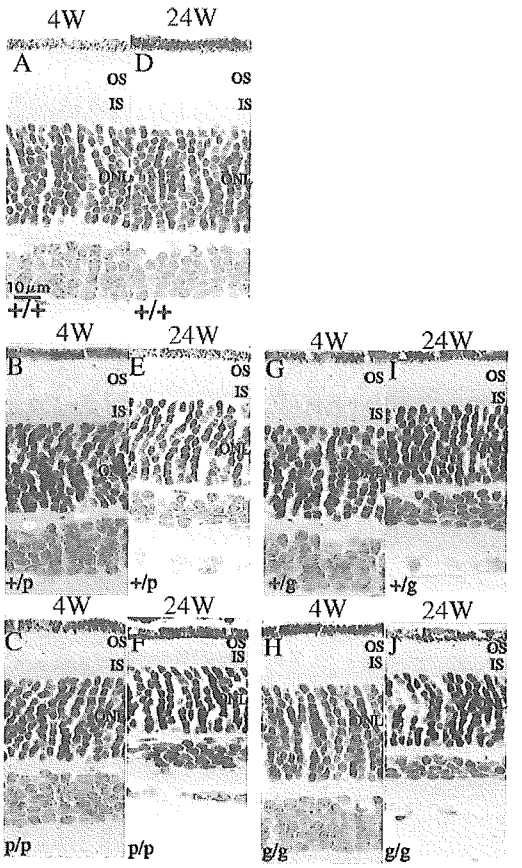

図 2　各遺伝子型マウスの網膜切片
A 4 週齢野生型 B 4 週齢 p 型ヘテロ C 4 週齢 p 型ホモ D 24 週齢野生型 E 24 週齢 p 型ヘテロ F 24 週齢 p 型ホモ G 4 週齢 g 型ヘテロ H 4 週齢 g 型ホモ I 24 週齢 g 型ヘテロ J 24 週齢 g 型ホモ

D. 考察

これまでの研究から、視細胞においてアクチン繊維ネットワークは細胞骨格の支持や外節板の成長、更にはロドプシン等の、外節細胞膜の構成成分の輸送に関わっており、また、FSCN2 遺伝子産物はアクチン繊維の

結合・束状化活性を有していることが示唆されている。それ故、FSCN2$^{p/p}$, FSCN2$^{g/g}$各マウス網膜での所見から、FSCN2 遺伝子産物の異常によりこれらの構造の形成が障害され、ひいては視細胞の機能異常につながることが示唆された。また、ヒトでの発症形式としては FSCN2 遺伝子産物の haplo-insufficiency によるものであると推定された。

また、網膜電図での結果より、FSCN2 遺伝子変異マウスでの視細胞変性はヒトの網膜色素変性症に似た変化を呈すると考えられた。

E. 結論

FSCN2 遺伝子異常では、FSCN2 遺伝子産物の haplo-insufficiency により外節板の形成が阻害され、ヒトの常染色体優性網膜色素変性症に類似した視細胞変性が引き起こされると考えられた。

F. 健康危険情報

なし

G. 研究発表

1. 論文発表

1. Yokokura S et al: Targeted disruption of FSCN2 gene induces retinopathy in mice. Invest Ophthalmol Vis Sci. 46: 2905-2915, 2005.

2. 学会発表

1. 横倉俊二　他：FSCN2 遺伝子変異マウスの開発とその網膜の解析. 第 109 回 日本眼科学会総会、京都市、2005
2. Yokokura S et al: Targeted disruption of FSCN2 gene induces retinopathy in mice. The Association for Research in Vision and Ophthalmology (ARVO), Fort Lauderdale, Florida, 2005

H. 知的財産権の出願・登録状況

1. 特許取得

なし

2. 実用新案登録

なし

3. その他

なし

I. 参考文献

1. Saishin Y et al: Retinal fascin: functional nature, subcellular distribution, and chromosomal localization. Invest Ophthalmol Vis Sci 41: 2087-2095, 2000.
2. Wada Y et al: Mutation of human retinal ascin gene (FSCN2) causes autosomal dominant retinitis pigmentosa. Invest Ophthalmol Vis Sci 42: 2395-2400, 2001.
3. Wada Yet al: Autosomal dominant macular degeneration associated with 208delG in FSCN2 gene. Arch Ophthalmol 121: 1613-1620, 2003.
4. Yokokura S et al: Targeted disruption of FSCN2 gene induces retinopathy in mice. Invest Ophthalmol Vis Sci, 46: 2905-2915, 2005.

Targeted Disruption of *FSCN2* Gene Induces Retinopathy in Mice

Shunji Yokokura,[1] *Yuko Wada,*[1] *Shigeyasu Nakai,*[2] *Hajime Sato,*[1] *Ryoji Yao,*[2] *Hitomi Yamanaka,*[2] *Sioko Ito,*[2] *Yoshiko Sagara,*[1] *Mayumi Takahashi,*[1] *Yukie Nakamura,*[1] *Makoto Tamai,*[1] *and Tetsuo Noda*[2,3,4]

Purpose. To investigate the morphology and function of photoreceptors in mice with mutation of the *FSCN2* gene.

Methods. A mouse line was generated carrying the 208delG mutation (point mutation, or p-type) and another with replacement of exon 1 by the cDNA of a green fluorescent protein (GFP knock-in, or g-type). The expression of retinal mRNA was determined by reverse transcription (RT)-polymerase chain reaction (PCR) and in situ hybridization performed on retinal sections. Morphologic analyses of the retinas were performed by light microscopy (LM) and transmission electron microscopy (TEM) and functional analyses by electroretinogram (ERG).

Results. mRNA of *FSCN2* was not detected in the retinal mRNA extracted from $FSCN2^{p/p}$ and $FSCN2^{g/g}$ mice. Both $FSCN2^{+/p}$ and $FSCN2^{+/g}$ mice had progressive photoreceptor degeneration with increasing age detected by LM and structural abnormalities of the outer segment (OS) detected by TEM. Both $FSCN2^{+/p}$ and $FSCN2^{+/g}$ mice had depressed rod and cone ERGs that worsened with increasing age.

Conclusions. These results indicate that haploinsufficiency of the *FSCN2* gene may hamper maintenance and/or elongation of the OS disks and result in photoreceptor degeneration, as in human autosomal dominant retinitis pigmentosa. (*Invest Ophthalmol Vis Sci.* 2005;46:2905-2915) DOI:10.1167/iovs.04-0856

Retinitis pigmentosa (RP) is an ocular disease causing severe loss of central and peripheral vision.[1,2] The main clinical features of RP are early onset of night blindness followed by a decrease in the electroretinogram (ERG), constriction and gradual loss of visual fields, and a decrease in visual acuity. There is no effective treatment for the disease, although some researchers are studying gene therapy[3] or the implantation of an artificial retina.[4]

RP can have an autosomal dominant (ADRP), autosomal recessive (ARRP), or X-linked (XLRP) inheritance pattern. Thirteen genes that cause ADRP have been mapped and cloned by genetic analyses.[5] Approximately 30% to 40% of patients with ADRP in the United States have mutations in the rhodopsin or *RP1* gene.[5]

Macular degeneration (MD) is characterized by a reduction of visual acuity, abnormal color vision, and a central scotoma.[6] Hereditary MD can have an autosomal dominant (ADMD) or autosomal recessive (ARMD) inheritance pattern. To date, seven genes that lead to MD have been cloned and mapped.[5] There is also no effective treatment for hereditary MD, although some therapeutic procedures are being tried.[7,8]

Wada et al.[9,10] reported that mutations in the retinal fascin gene (*FSCN2*) were the cause of ADRP (14 patients from 4 unrelated families) and ADMD (5 patients from 2 unrelated families) in a Japanese cohort. All affected members were heterozygous for the 208delG mutation. The human *FSCN2* gene is located at q25 on chromosome 17[11] and encodes 516 amino acids.[12] It is expressed specifically in the photoreceptors of the retina,[12,13] and its products induce actin-binding and bundling.[12] These functions indicate that the *FSCN2* gene plays an important role in the morphogenesis of photoreceptors, especially in the outer segments (OS).

We generated a mouse line carrying the 208delG mutation (point mutation, or p-type) and another with a replacement of exon 1 by the cDNA of a enhanced green fluorescein protein (GFP knock-in, or g-type), to investigate a possible mechanism of the retinopathy in patients with mutations of the *FSCN2* gene. Heterozygotes with both types of mutations showed RP-like photoreceptor degeneration with increasing age but did not show MD-like changes. Retinal mRNA extracted from $FSCN2^{p/p}$ mice lacked mRNA of *FSCN2*. These results indicate that haploinsufficiency[14] of the *FSCN2* gene may cause ADRP as in human 208delG heterozygotes.

Materials and Methods

Animals

All animal procedures adhered to the ARVO Statement for the Use of Animals in Ophthalmic and Vision Research.

Gene Targeting

The *FSCN2* genomic clone was obtained from a 129SVJ mouse library. A fragment lacking a guanine at nucleotide 208 of the mouse *FSCN2* gene, corresponding to the human 208delG mutation of *FSCN2*, was generated by polymerase chain reaction (PCR). Mixtures of 256-bp PCR product with one primer pair (5′-ACAAGACAGAGGGAGGCAGCATTG-3′, p21, and 5′-CTCTCTGCAGTAGGTAGCGGTCGGCAT-3′, p18) and an 186-bp PCR product with the other primer pair (5′-CGACCGCTACCTACTGCAGAGAGCTTTG-3′, p19, and 5′-ATCCATCTCACAGGCCACACGTCCA-3′, p30) were used as templates to create a 419-bp fragment lacking guanine, with the sense primer p21 and the antisense primer p30. The fragment replaced the *Bst*XI/*Sma*I region (284 bp) on the 5′ genomic flanking sequence (10.5 kb) subcloned

From the Departments of [1]Ophthalmology and [3]Molecular Genetics, Tohoku University School of Medicine, Miyagi, Japan; the [2]Department of Cell Biology, Japanese Foundation for Cancer Research (JFCR) Cancer Institute, Tokyo, Japan; and the [4]Mouse Functional Genomics Research Group, Institute of Physical and Chemical Research (RIKEN), Genomic Sciences Center, Yokohama, Kanagawa, Japan.

Submitted for publication July 22, 2004; revised December 1, 2004, and February 28, 2005; accepted March 8, 2005.

Disclosure: **S. Yokokura**, None; **Y. Wada**, None; **S. Nakai**, None; **H. Sato**, None; **R. Yao**, None; **H. Yamanaka**, None; **S. Ito**, None; **Y. Sagara**, None; **M. Takahashi**, None; **Y. Nakamura**, None; **M. Tamai**, None; **T. Noda**, None

The publication costs of this article were defrayed in part by page charge payment. This article must therefore be marked "*advertisement*" in accordance with 18 U.S.C. §1734 solely to indicate this fact.

Corresponding author: Shunji Yokokura, Department of Ophthalmology, Tohoku University School of Medicine, 1-1 Seiryo-machi, Aoba-Ku, Sendai, Miyagi 980-0873, Japan; yokokura@oph.med.tohoku.ac.jp.

into the *Eco*RI and *Kpn*I sites of a vector (pBlueScript; Stratagene, La Jolla, CA). The floxed pMC1-neo poly(A) fragment, the 3′ genomic flanking sequence (2.3 kb), and the DT-A (diphtheria toxin A-chain) fragment were ligated at the 3′ end of this fragment. An 853-bp fragment was created in which exon 1 was replaced by the cDNA of enhanced green fluorescein protein (EGFP; BD-Clonetech, Palo Alto, CA) in frame, by PCR. The mixture of a 118-bp PCR product obtained with one primer pair (5′-AGATAAACAGATCTGGGCCTCAGG-3′, p17, and 5′-CCCTTGCTCACCATCTTTGAGGCTAGCCACGT-3′, pG2) and a 762-bp PCR product with the other primer pair (5′-GCTAGCCTCAAA-GATGGTGAGCAAGGGCGAGGA-3′, pG1, and 5′GGCTGATTAT-GATCTAGAGTCGCG-3′, pG6) was used as a template to create the 853-bp fragment, obtaining EGFP with the sense primer p17 and the antisense primer pG6. The fragment was replaced with the *Nhe*I/*Kpn*I region (1521 bp) on the 3′ genomic flanking sequence (2.7 kb) and ligated DT-A fragment at the 5′ end of this fragment. Finally, we ligated pMC1-neo poly(A) and 5′ genomic flanking sequence (8.8 kb) on the 3′ end of the fragment. Each targeting vector was linearized with the *Not*I site and electroporated into J1 embryonic stem (ES) cells. Twelve clones of 120 G418-resistant clones that had a point mutation (p-type) and 17 clones of 140 G418-resistant clones in which exon 1 was replaced by EGFP (g-type) underwent homologous recombination, as determined by Southern blot analysis. Two p-type-positive clones and one g-type-positive clone were injected into C57BL/6 blastocysts, resulting in the birth of male chimeric mice. Germline transmission of the disrupted *FSCN2* alleles was determined by mating these chimeric mice with C57BL/6 females.

RT-PCR Analysis

Poly(A) mRNA was extracted from retinas of 8-week-old wild-type, heterozygous, and homozygous mice with a kit (FastTrack; Invitrogen, Carlsbad, CA). cDNA synthesis and PCR were performed with a cDNA cycle kit (Invitrogen). Two primer pairs were used for the detection of the wild-type *FSCN2* mRNA. Primers for detecting the 343-bp fragment were 5′-GCTACGTGCACCTGTGCCTTCAGG-3′ (p23) and 5′-TACCAG-CACCACCTGTGGGTGACT-3′ (p24) and primers for detecting the 720-bp fragment were 5′-AGGATGAACTCTTCGACCTGGAGC-3′ (p11) and 5′-CTTCCCCCACAGGCAGGTCTGCAT-3′ (p32). The primer pair for β-actin detection as control was 5′-CCTTCAACACCCCAGCCATG-3′ and 5′-TGCGCTCAGGAGGAGCAATG-3′.

In Situ Hybridization

Wild-type, *FSCN2*$^{+/p}$, and *FSCN2*$^{p/p}$ mice were perfused with 4% paraformaldehyde (PFA) in PBS, and the eyes were enucleated and fixed overnight at 4°C with 4% PFA in PBS. The eyes were rinsed in PBS three times, passed through a sucrose gradient (10%, 20%, and 30% in PBS) and then incubated in 30% sucrose-optimal cutting temperature (OCT) compound (1:1) overnight at 4°C. The eyes were embedded in a 1:1 mixture of 30% sucrose/OCT compound, and sectioned at 12-μm thickness with a cryostat. RNA in situ hybridization was performed by a protocol modified from that described earlier.[15] Riboprobes (619 bp) were synthesized by using wild-type murine retinal cDNA and a specific primer pair (5′-TCGGAACTCAAAGAGGAAATCTTC-3′ and 5′-AG-GATGAACTCTTCGACCTGGAGC-3′).

Examination of GFP in Retinal Sections

The same procedures were used as in the in situ hybridization, to prepare retinal sections. Embedded eyes of wild-type *FSCN2*$^{g/g}$ mice were sectioned at 6-μm thickness with a cryostat. Sections were counterstained by 4′,6-diamino-2-phenylindole (DAPI) for 20 minutes, washed by PBS three times, and examined.

Retinal Histology

Specimens were perfused and fixed with 2% PFA plus 2.5% glutaraldehyde (GA) in cacodylate-buffer for 1 week. The eyes were rinsed in PBS twice and were dehydrated in a graded ethanol series. The specimens were infiltrated with mixtures of chloroform and paraffin three times and then embedded in paraffin. The sections were cut at 3 μm along the vertical meridian and stained with hematoxylin and eosin. The thicknesses of the outer nuclear (ONL) and inner nuclear (INL) layers, the number of cells in the ONL and INL, and the length of the OS were measured by light microscopy, as described.[16] The measurements were made at several equidistant loci, beginning at the optic nerve head.

Transmission Electron Microscopy

Eyes were perfused and fixed with 2% PFA and 2.5% GA in cacodylate-buffer for 1 week. The anterior segments were removed, and the eyecups were rinsed in 0.1 M PB five times. The eyecups were then osmicated for 1 hour in 2% aqueous solution of osmium tetroxide and dehydrated through ascending ethanol (50%–100%, 10 min/step). After five changes of 100% ethanol, the specimens were passed through propylene oxide twice and left overnight in a 1:1 mixture of propylene oxide and araldite. The specimens were embedded and cured in pure Epon for 6 hours at 80°C. Ultrathin sections were cut with a microtome (EM-Ultracut; Leica, Deerfield, IL), and the sections (80–90 nm) were collected on polyvinyl formal (Formvar)-coated 100-mesh copper grids (SPI, West Chester, PA, and examined with an electron microscope at 80 kV (JEM-1010; JEOL, Tokyo, Japan).

Electroretinograms

For the dark-adapted ERGs, the animals were dark-adapted overnight and prepared for the recordings in dim red light. After dark adaptation for an additional 30 minutes, they were anesthetized by intramuscular injections of xylazine (13 mg/kg) and ketamine (86 mg/kg). The pupils were dilated with 0.1% phenylephrine HCl. The body temperature was maintained close to 38°C with a heating pad. ERGs were recorded with a 1-mm silver-silver chloride wire-loop electrode placed on the cornea, which was anesthetized by topical 1% tetracaine. A stainless-steel needle was inserted subcutaneously on the nose as the reference electrode. Signals were amplified 10,000 times and band-pass filtered from 0.1 to 1000 Hz. The mice were placed in a Ganzfeld bowl, and single-flash ERGs were recorded with increasing light intensities from 0.01 to 10 cd/m^2 in equal-size, logarithmic steps. Five responses were averaged at each intensity, and the interstimulus interval increased from 10 seconds for 0.01 and 0.1 cd/m^2 and 60 seconds for 1 and 10 cd/m^2. Light-adapted ERGs were recorded with 1 and 10 cd/m^2-flashes on a background of 43 cd/m^2, to suppress rod responses after 20 minutes of exposure to the background light.

Results

Generation of *FSCN2* Knockout and Knock-in Mice

A guanine was deleted from nucleotide 208 of the mouse *FSCN* 2 gene, the same deletion that occurs in humans with ADRP or ADMD, for a single-base deleted allele with homologous recombination (Fig. 1A). In another line, exon 1 of the *FSCN2* was displaced by GFP for an exon 1-null allele with the same method (Fig. 2A). Each type of mouse (point mutation [p-type], and GFP knock-in [g-type]) was crossed with CAG-Cre transgenic mice to remove the neomycin-resistant genes (Figs. 1A and 2A). The single-base deletion and displacement of exon 1 were confirmed by Southern blot analyses (Figs. 1B, 2B). For LM, transmission electron microscopy (TEM), and ERGs, mice without neomycin-resistant genes were used. *FSCN2*$^{+/p}$ neo(+) and -(−), *FSCN2*$^{p/p}$ neo(+) and -(−), *FSCN2*$^{+/g}$ neo(+) and -(−), and *FSCN2*$^{g/g}$ neo(+) and -(−) mice were morphologically normal, viable, and fertile.

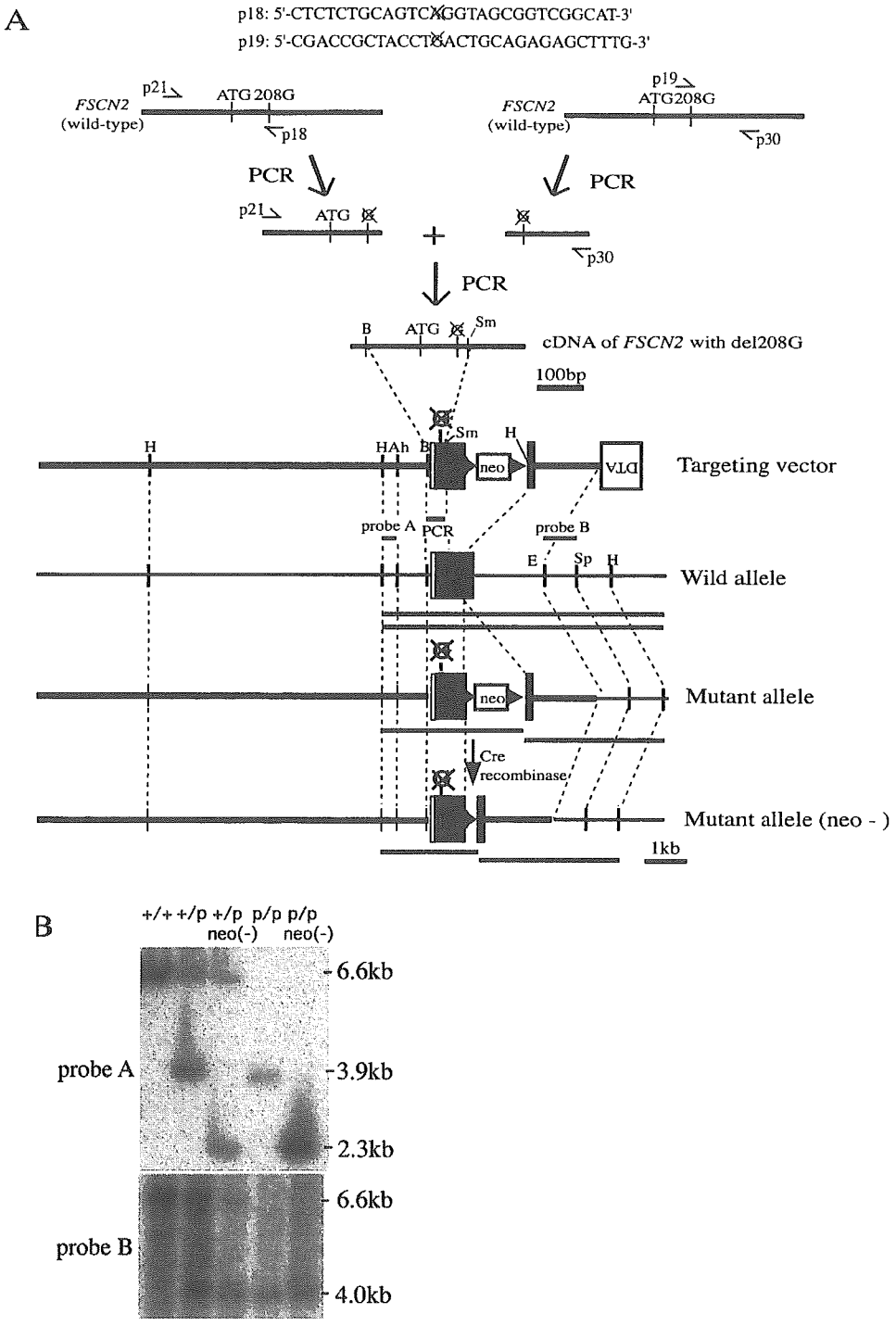

FIGURE 1. (**A**) Construction of the targeting vector for single-base deletion. *Filled boxes*: exon 1 of the *FSCN2* gene; *filled triangles*: loxP sequences. PCR, an artificial sequence containing deletion by PCR of a guanine that is located at the same position as human nucleotide 208G. A 0.7-kb, 3′ probe (*Eco*RI-*Spe*I fragment, probe B) detects a 6.6- and a 4.0-kb *Hin*dIII fragment in wild-type and the targeted allele neo(+), respectively. A 0.5-kb, 5′ probe (*Hin*dIII-*Aha*I fragment, probe A) detects a 2.3-kb *Hin*dIII fragment in the targeted allele neo(−). G and C with *red* Xs represent the deleted guanine and cytosine, respectively. neo, neomycin-resistant gene driven by the thymidine kinase promoter diphtheria toxin A-chain (DT-A) gene; H, *Hin*dIII; Ah, *Aha*I; B, *Bst*XI; Sm, *Sma*I; Sp, *Spe*I; G (with X), the deleted guanine. (**B**) Southern blot of *Hin*dIII digested mouse-tail genomic DNA. Probe B detects 6.6- and 4.0-kb fragments corresponding to the wild-type and the single-base deleted allele, respectively. Probe A detects a 2.3-kb fragment corresponding to single-base deleted allele neo(−).

In the 8-week-old *FSCN2*$^{g/g}$ neo(−) retina, green fluorescence was detected in the photoreceptors, although no signals were observed in 8-week-old, wild-type retinas (Figs. 2C–H).

Expression of *FSCN2* mRNA in *FSCN2* Mutant Mice

RT-PCR was performed to evaluate the expression of mouse *FSCN2* mRNA in samples extracted from 8-week-old wild-type, *FSCN2*$^{+/p}$ neo(+) and -(−), *FSCN2*$^{p/p}$ neo(+) and -(−), *FSCN2*$^{+/g}$ neo(+), and -(−), and *FSCN2*$^{g/g}$ neo(+) and -(−) mice (Fig. 3A). The mRNA of *FSCN2* was not detected with the pair of primers (p11 and p32) that detected cDNA of *FSCN2* downstream of the GFP poly(A) sequence in *FSCN2*$^{g/g}$ neo(+) and -(−) mice (Fig. 3B). In *FSCN2*$^{p/p}$ neo(+) and -(−) mice, the mRNA of *FSCN2* was also not observed with p11 and p32 and was not detected with another pair of primers (p23 and p24) that detected cDNA of *FSCN2* downstream of the deleted guanine (Fig. 3B).

In situ hybridization with a cRNA riboprobe specific for the 3′ end of the mRNA of *FSCN2* was performed on retinal sections of 8-week-old wild-type and *FSCN2*$^{p/p}$ neo(−) mice (Fig. 3A). In the wild-type retina, hybridization signals for mRNA of mouse *FSCN2*

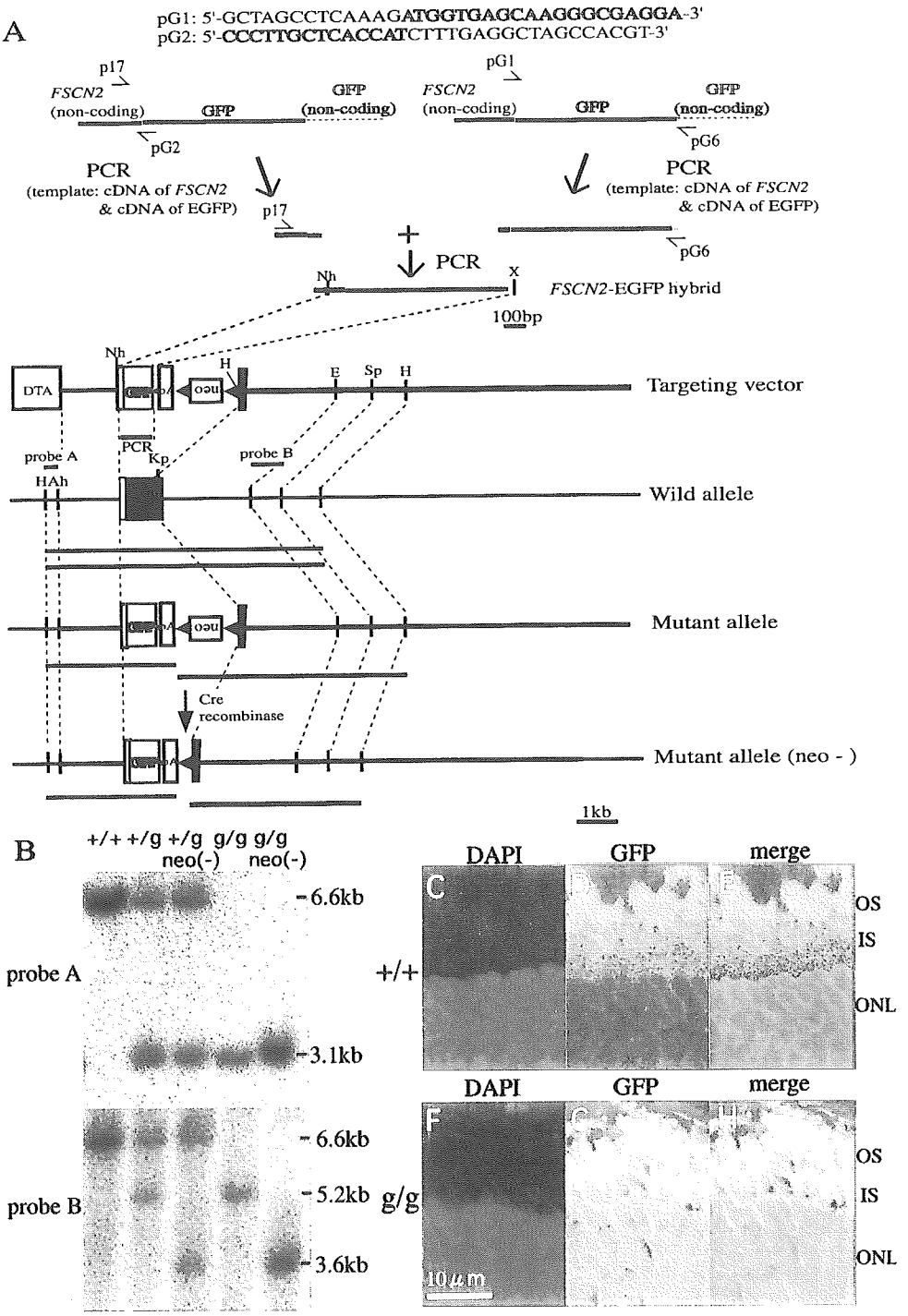

FIGURE 2. (A) Construction of a targeting vector for the disruption of almost all of exon 1. PCR, the artificial sequence in which cDNA of GFP replaced exon 1 of *FSCN2* in frame, by PCR. Probe A detects 6.6- and 3.1-kb *Hin*dIII fragments in wild-type and targeted allele neo(+), respectively. Probe B detects a 3.6-kb *Hin*dIII fragment in targeted allele neo(−). *Green symbols* and *lines:* cDNA of EGFP. pA, poly(A) sequence derived from cDNA of bovine growth hormone; Nh, *Nhe*I; X, *Xba*I; E, *Eco*RI. (B) Southern blot of *Hin*dIII-digested mouse-tail genomic DNA. Probe A detects 6.6- and 3.1-kb fragments corresponding to the wild-type and the exon 1-null allele, respectively. Probe B detects a 3.6-kb fragment corresponding to the exon 1-null allele neo(−). (C–H) Fluorescence of GFP in retinal sections in 8-week-old mice. (C) Wild-type retina with DAPI staining. (D) Background fluorescence in wild-type retina. (E) Merged image of (C) and (D). (F) $FSCN2^{g/g}$ neo(−) retina with DAPI staining. (G) Fluorescence image in $FSCN2^{g/g}$ neo(−) retina. Green fluorescence is shown in the photoreceptors. (H) Merged image of (F) and (G).

were found in the inner segment (IS) and the ONL, but no signal was observed in the OS of the photoreceptors and in other layers of the retina (Fig. 3D). Signals for the mRNA of *FSCN2* were not detected in any layers, including the IS and the ONL in $FSCN2^{p/p}$ neo(−) retina (Fig. 3E).

Light Microscopic Analysis of Retina of *FSCN2* Mutant Mice

The length of the OS, thickness of the ONL, and thickness of the INL were measured in retinal sections from 4-, 8-, 16-, and 24-week-old wild-type, $FSCN2^{+/p}$ neo(−), and $FSCN2^{p/p}$ neo(−) mice, and the number of nuclei in the ONL and INL were counted as described.[16] At 4 weeks of age, the OS in the central retinal region of $FSCN2^{+/p}$ neo(−) mice were shorter than in the wild-type ($P < 0.05$), and the ONL was slightly thinner ($P < 0.05$), with fewer nuclei than in the wild-type mice (Figs. 4A, 4B, 5). $FSCN2^{p/p}$ neo(−) mice at the same age had much shorter OS than did the $FSCN2^{+/p}$ neo(−) mice, but the thickness and cell counts in the ONL were comparable to those in the $FSCN2^{+/p}$ neo(−) mice (Figs. 4B, 4C, 5). The thickness of the INL of $FSCN2^{+/p}$ neo(−) and $FSCN2^{p/p}$ neo(−) mice was almost the same as in wild-type mice, and cell counts in the INL of $FSCN2^{+/p}$ neo(−) and $FSCN2^{p/p}$ neo(−) mice were similar to wild-type (Figs. 4A–C, 6).

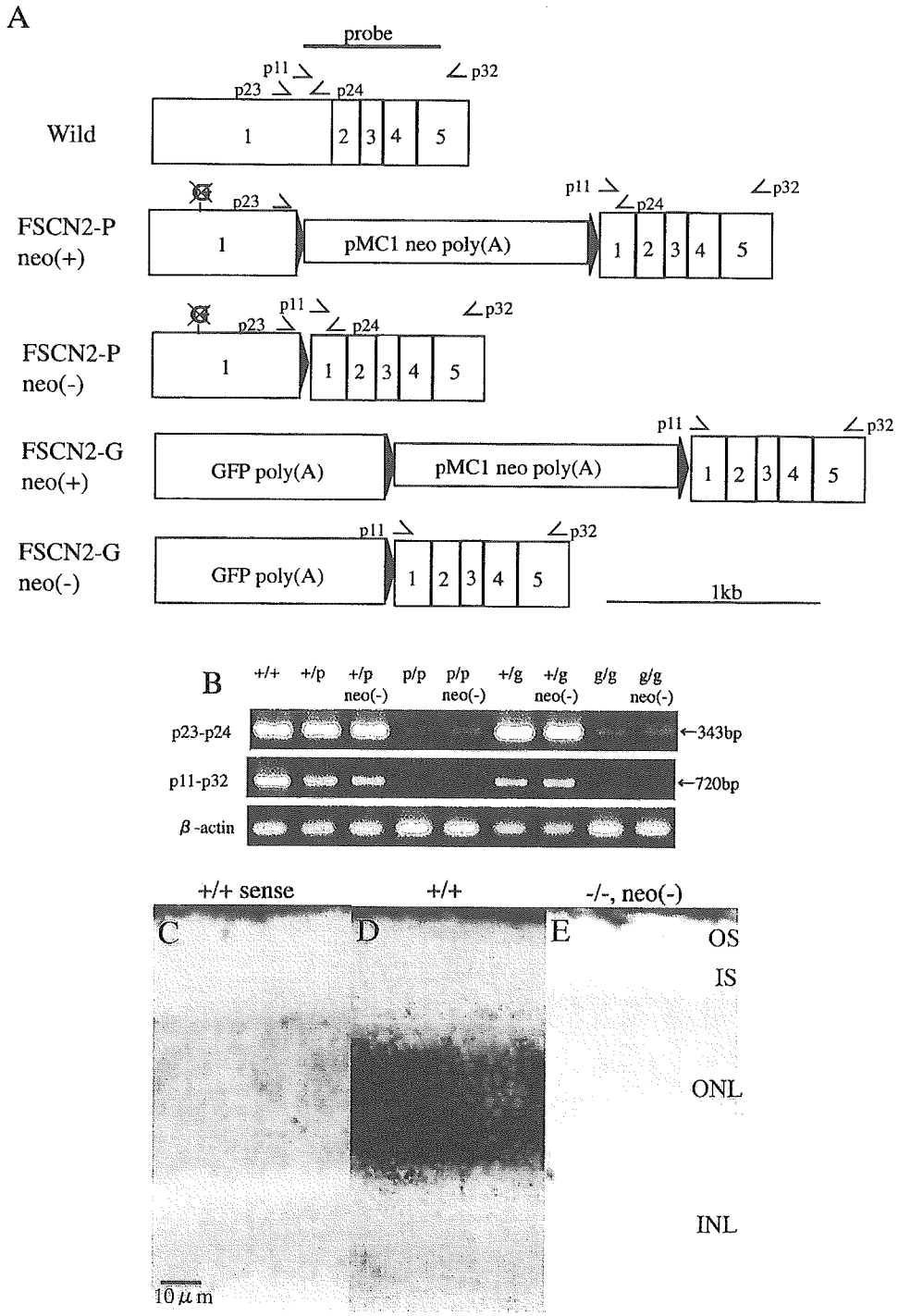

FIGURE 3. (**A**) Primers for RT-PCR and a riboprobe for in situ hybridization. *Filled triangles*: lox-P sequences. Probe, riboprobe for in situ hybridization; p11, p23, p24, and p32, primers for RT-PCR; G (with *red* X), the deleted guanine. (**B**) RT-PCR of retinal RNA isolated from 8-week-old mice. *FSCN2* primers are from exons 1 and 5, amplifying a 343-bp (p23-p24) and a 720-bp (p11-p32) product of wild-type. mRNA of $FSCN2^{p/p}$ neo(+) and -(−) were not detected with both pairs of primers. mRNA of $FSCN2^{g/g}$ neo(+) and -(−) also were not observed with both pairs of primers. β-Actin primers were used as the control. (**C–E**) In situ hybridization with *FSCN2* riboprobes in retinal sections of 8-week-old mice. Retinal section of (**C**) wild-type with the sense probe as the control and (**D**) wild-type with the antisense probe. Hybridization signals are shown in the IS and ONL of photoreceptors. There was no signal in other layers, including the OS of photoreceptors. (**E**) Retinal section of $FSCN2^{p/p}$ neo(−) with antisense probe. No signal was observed in all layers.

At 24-week, the $FSCN2^{+/p}$ neo(−) mice had significantly shorter OS ($P < 0.01$), thinner ONL ($P < 0.01$), and thinner INL ($P < 0.05$), with reduced cell counts in the ONL and the INL compared with those in the wild-type mice (Figs. 4D, 4E, 5A–C, 6). The $FSCN2^{p/p}$ neo(−) mice at the same age had significantly shorter OS and a significantly thinner ONL and INL with fewer nuclei than the $FSCN2^{+/p}$ neo(−) mice (Figs. 4E, 4F, 5, 6). In the p-type neo(+) and -(−) mice, the difference in the length of the OS and thickness of the ONL and the number of nuclei in the ONL were not significantly different (data not shown).

The retinal morphologies of the $FSCN2^{+/g}$ neo(−) and $FSCN2^{g/g}$ neo(−) mice were comparable to that of $FSCN2^{+/p}$ neo(−) and $FSCN2^{p/p}$ neo(−) mice, respectively (Figs. 4G-J 5, 6). No significant differences in the length of the OS, thickness of the ONL, thickness of the INL, or the number of nuclei in the ONL and INL were observed between the g-type neo(+) and -(−) mice (data not shown).

TEM Analysis of Retina of *FSCN2* Mutant Mice

The ultrastructure of the retinas, especially the OS of the wild-type, $FSCN2^{+/p}$ neo(−), and $FSCN2^{p/p}$ neo(−) mice, was examined by TEM. At 4 weeks, the OS of $FSCN2^{+/p}$ neo(−) retina appeared very similar to that of wild-type mice, but the

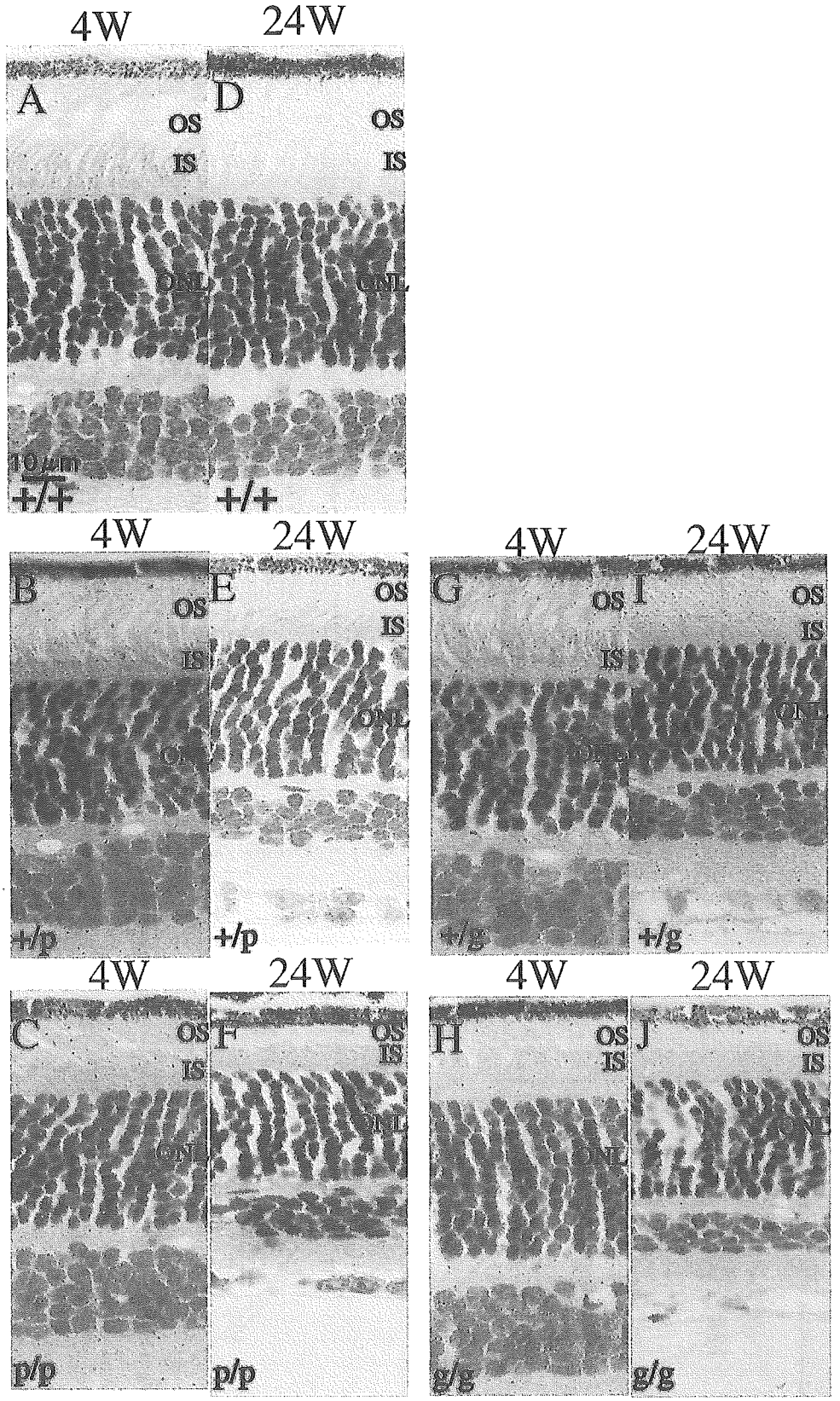

FIGURE 4. (A–C) Sections of central retina (relative distance from optic nerve head is 0.2) of 4-week-old (A) wild-type and (B) *FSCN2*$^{+/p}$ neo(−) mice. The OS were slightly shorter than those of wild-type, and the ONL was slightly thinner, with fewer nuclei than in the wild-type. The thickness of the INL was almost the same as in the wild-type. (C) Retinal section of 4-week-old *FSCN2*$^{p/p}$ neo(−) mouse. The *FSCN2*$^{p/p}$ neo(−) retina had much shorter OS and thinner ONL than did the wild-type. The thickness of the INL was very similar to that in the wild-type. (D–F) Sections of the central retina of 24-week-old (D) wild-type and (E) *FSCN2*$^{+/p}$ neo(−) mice. The *FSCN2*$^{+/p}$ mice had significantly shorter OS and thinner ONL and INL, with reduced cell counts in the ONL and INL than did the wild-type. (F) Retinal section of 24-week-old *FSCN2*$^{p/p}$ neo(−) mouse. The *FSCN2*$^{p/p}$ neo(−) mice had significantly shorter OS and thinner ONL and INL, with fewer nuclei than did the *FSCN2*$^{+/p}$ neo(−). (G–J) Retinal sections of central retina from 4-week-old (G) *FSCN2*$^{+/g}$ neo(−) and (H) *FSCN2*$^{g/g}$ neo(−) mice and 24-week-old (I) *FSCN2*$^{+/g}$ neo(−) and (J) *FSCN2*$^{g/g}$ neo(−) mice. Hematoxylin-eosin; magnification, ×400.

OS of *FSCN2*$^{p/p}$ neo(−) photoreceptors were extremely bent (Figs. 7A–C). There was no significant difference in the alignment of OS discs between wild-type and *FSCN2*$^{+/p}$ neo(−) mice (Figs. 7K, 7L), but misalignment of OS discs was observed at the OS of *FSCN2*$^{p/p}$ neo(−) mice, especially near the distal end of connecting cilium (Fig. 7M).

At 24 weeks, the retinas of *FSCN2*$^{+/p}$ neo(−) and *FSCN2*$^{p/p}$ neo(−) mice had considerably shorter OS (Figs.

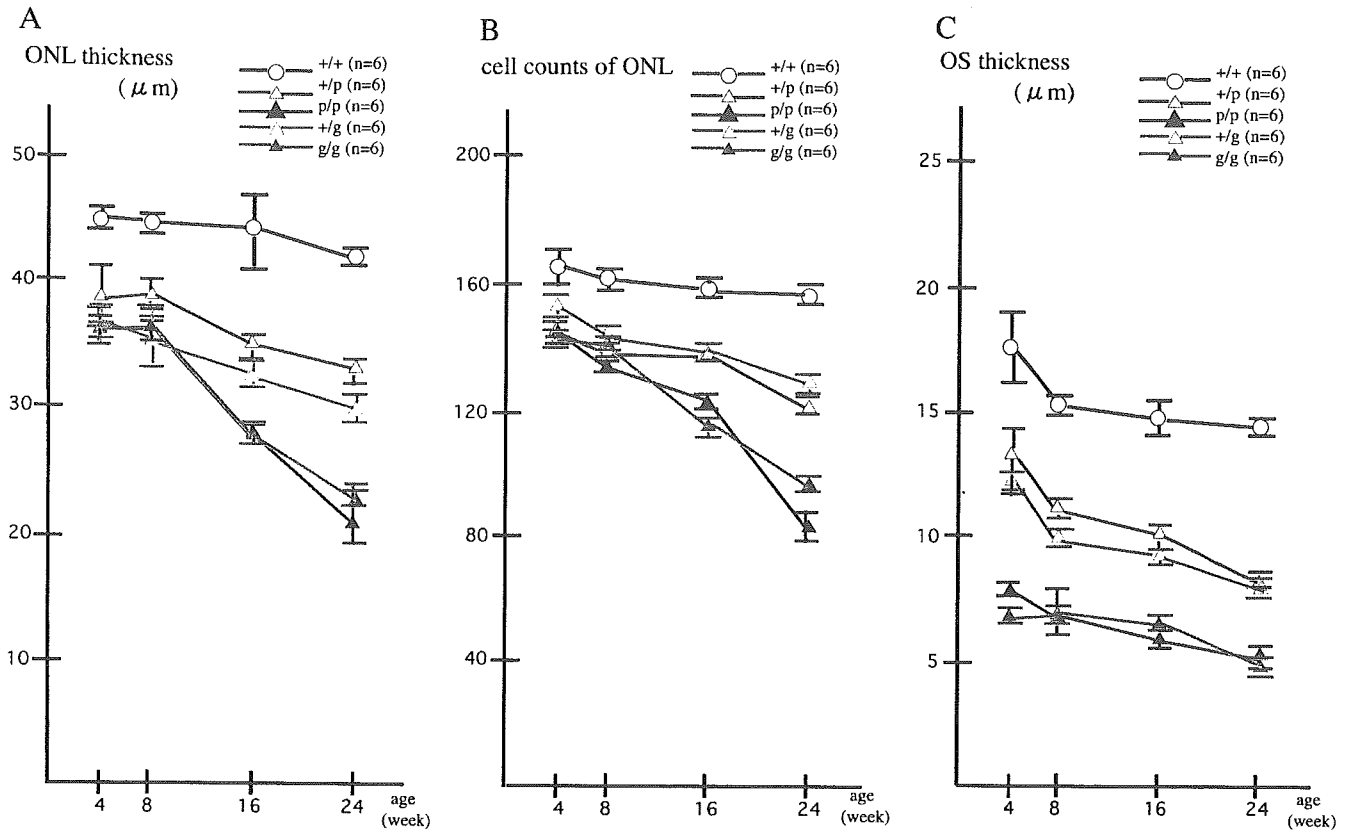

FIGURE 5. Time course of the changes in the central retina (relative distance from the optic nerve head is 0.2) of (**A**) thickness of the ONL, (**B**) nuclei in the ONL, and (**C**) the length of the OS in the central retina. In both mutant homozygous mice and mutant heterozygous mice, the OS were shorter, the ONL were thinner, and the number of the nuclei in the ONL decreased with increasing age. Data are the mean ± SEM. ++, wild-type; +/p, *FSCN2*$^{+/p}$; p/p, *FSCN2*$^{p/p}$; +/g, *FSCN2*$^{+/g}$; g/g, *FSCN2*$^{g/g}$; n = 6 for each genotype.

7D–F), agreeing with the LM analyses. Misalignment of OS discs was not observed in wild-type and *FSCN2*$^{+/p}$ neo(−) mice, but that of *FSCN2*$^{p/p}$ neo(−) mice was significantly stronger. The thickness and shape of the connecting cilium were not significantly different among all mice (Figs. 7N–P). There was no significant difference in the morphologic changes between the p-type neo(+) and -(−) mice (data not shown).

The ultrastructure of the retinas of *FSCN2*$^{+/g}$ neo(−) and *FSCN2*$^{g/g}$ neo(−) mice was comparable to that in *FSCN2*$^{+/p}$ neo(−) and *FSCN2*$^{p/p}$ neo(−) mice, respectively (Figs. 7G–J). No significant morphologic differences was

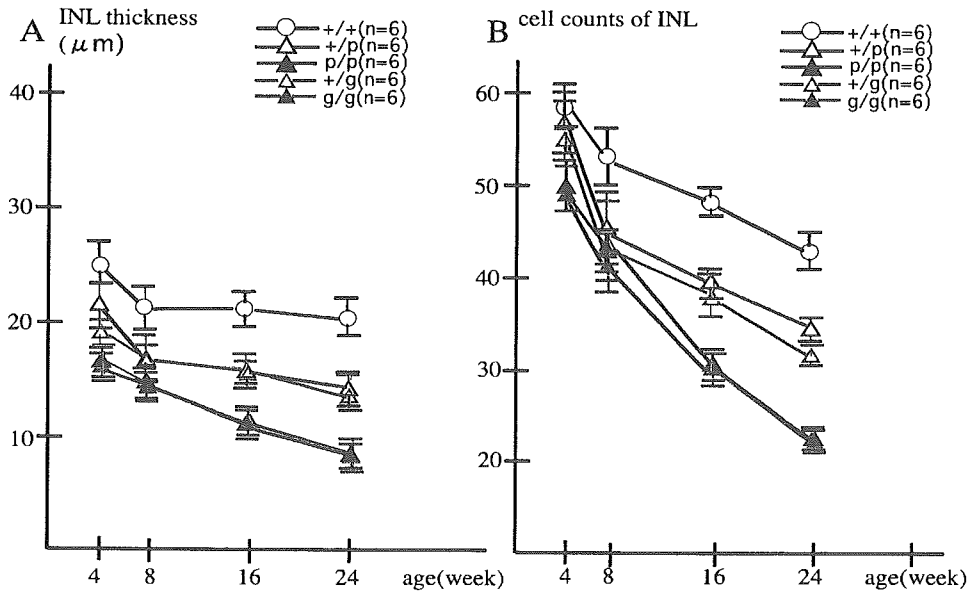

FIGURE 6. Time course of the changes in the central retina (relative distance from optic nerve head is 0.2) of (**A**) the thickness of the INL and (**B**) the nuclei in the INL. In both mutant homozygous and mutant heterozygous mice, the INL was thinner and the number of the nuclei in the INL decreased with increasing age. Data are the mean ± SEM. Labels for genotypes are as described in Figure 5; n = 6 for each genotype.

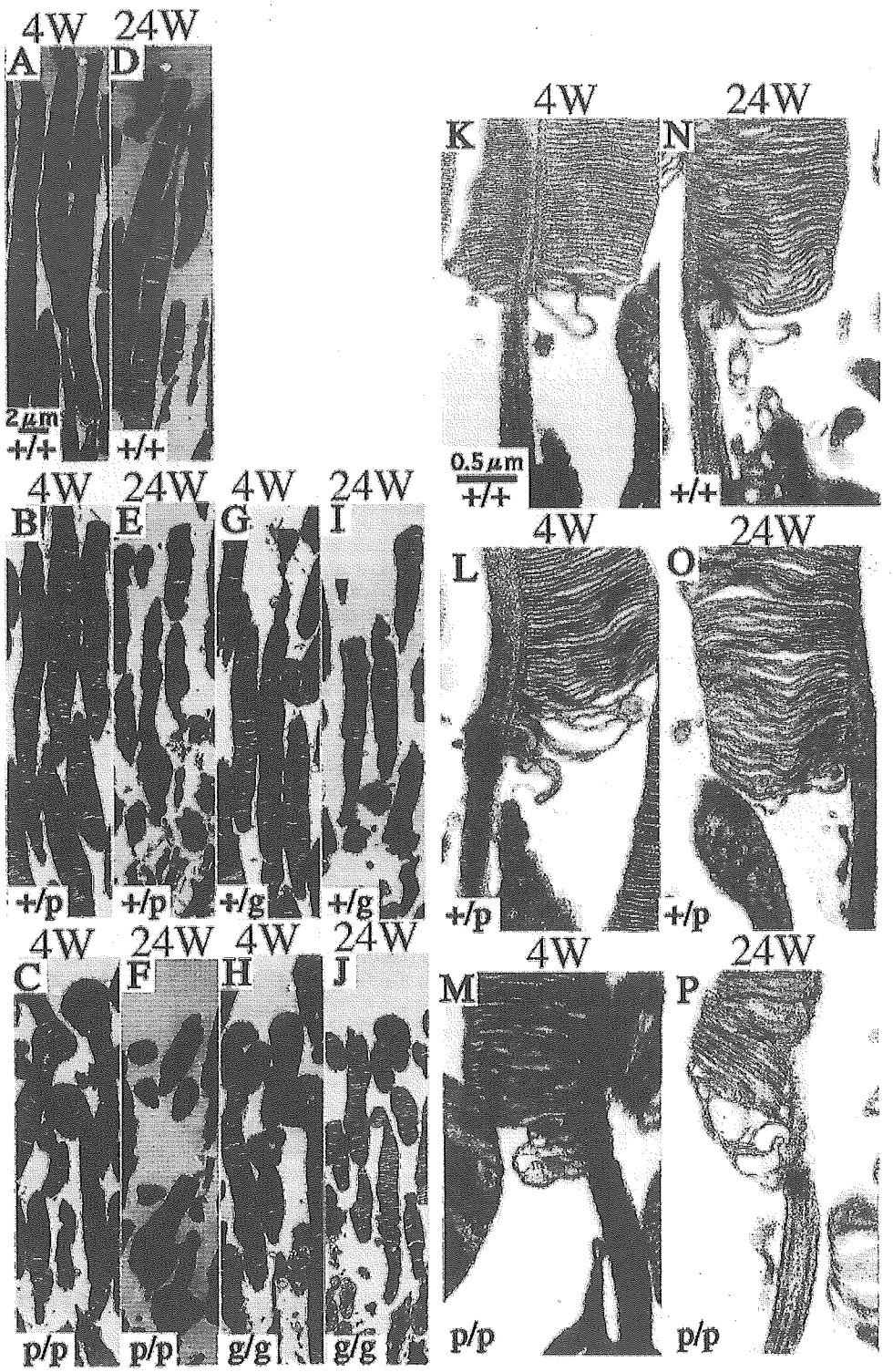

FIGURE 7. (**A–C**) Electron micrographs of the photoreceptors of 4-week-old (**A**) wild-type. (**B**) *FSCN2*$^{+/p}$ neo(−), and (**C**) *FSCN2*$^{p/p}$ neo(−) mice. The OS of the mice were extremely bent. (**D–F**) Electron micrographs of the photoreceptors of 24-week-old (**D**) wild-type, (**E**) FSCN2+/p neo(−), and (**F**) *FSCN2*$^{p/p}$ neo(−) mice. The OS of *FSCN2*$^{+/p}$ neo(−) and *FSCN2*$^{p/p}$ neo(−) mice were significantly shorter than those of the wild-type. (**G–J**) Electron micrographs of photoreceptors of 4-week-old (**G**) *FSCN2*$^{+/g}$ neo(−) and (**H**) *FSCN2*$^{g/g}$ neo(−) mice and of 24-week-old (**I**) *FSCN2*$^{+/g}$ neo(−) and (**J**) *FSCN2*$^{g/g}$ neo(−) mice. (**K–M**) Electron micrographs of the OS and connecting cilium of 4-week-old (**K**) wild-type, (**L**) *FSCN2*$^{+/p}$ neo(−), and (**M**) *FSCN2*$^{p/p}$ neo(−) mice. Misalignment of OS discs was observed at the distal end of the connecting cilium. (**N–P**) Electron micrographs of the OS and connecting cilium of 24-week-old (**N**) wild-type, (**O**) *FSCN2*$^{+/p}$ neo(−), and (**P**) *FSCN2*$^{p/p}$ neo(−) mice. Misalignment of OS discs of *FSCN2*$^{p/p}$ neo(−) mice was significantly more severe. Magnification: (**A–J**) ×6,900; (**K–P**) ×27,600. Scale bars: (**A–J**) 2 μm; (**K–P**) 0.5 μm.

observed between the g-type neo(+) and -(−) mice (data not shown).

ERGs of *FSCN2* Mutant Mice

ERGs were recorded in the wild-type, *FSCN2*$^{+/p}$ neo(−), and *FSCN2*$^{p/p}$ neo(−) mice under dark- and light-adapted conditions and at different ages to evaluate retinal function in vivo. At 4 weeks, the scotopic a- and b-wave amplitudes of *FSCN2*$^{+/p}$ neo(−) mice were similar to those in wild-type mice (Figs. 8A, 8B, 9A, 9B). But at 24 weeks, both the a- and b-waves were significantly smaller in the *FSCN2*$^{+/p}$ neo(−) mice than in the wild-type mice ($P < 0.01$; Figs. 8D, 8E, 9A, 9B). The ERGs of *FSCN2*$^{p/p}$ neo(−) mice were significantly smaller than those of *FSCN2*$^{+/p}$ neo(−) at 4 weeks and progressively decreased with increasing age (Figs. 8C, 8F, 9A, 9B).

At 4 weeks, the photopic b-wave amplitudes of *FSCN2*$^{+/p}$ neo(−) mice were comparable to those of the wild-type mice

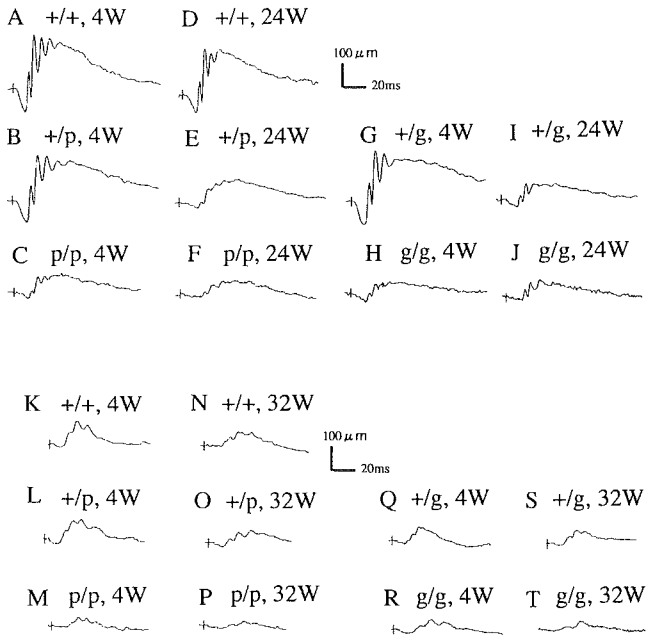

FIGURE 8. (**A–C**) Dark-adapted (scotopic) flash ERGs of 4-week-old (**A**) wild-type, (**B**) *FSCN2*$^{+/p}$ neo(−), and (**C**) *FSCN2*$^{p/p}$ neo(−) mice. The a- and b-wave amplitudes of *FSCN2*$^{p/p}$ neo(−) were significantly reduced compared with those of the wild-type. (**D–F**) Dark-adapted (scotopic) flash ERGs of 24-week-old (**D**) wild-type, (**E**) *FSCN2*$^{+/p}$ neo(−), and (**F**) *FSCN2*$^{p/p}$ neo(−) mice. The a- and b- wave amplitudes were reduced in both the *FSCN2*$^{p/p}$ neo(−) and the *FSCN2*$^{+/p}$ neo(−) mice. (**G–J**) Dark-adapted flash ERGs of 4-week-old (**G**) *FSCN2*$^{+/g}$ neo(−) and (**H**) *FSCN2*$^{g/g}$ neo(−) and of 24-week-old (**I**) *FSCN2*$^{+/g}$ neo(−) and (**J**) *FSCN2*$^{g/g}$ neo(−) mice. (**K–M**) Light-adapted ERGs of 4-week-old (**K**) wild-type, (**L**) *FSCN2*$^{+/p}$ neo(−), and (**M**) *FSCN2*$^{p/p}$ neo(−) mice. The b-wave amplitudes of *FSCN2*$^{p/p}$ neo(−) were significantly diminished. (**N–P**) Light-adapted ERGs of 32-week-old (**N**) wild-type, (**O**) *FSCN2*$^{+/p}$ neo(−), and (**P**) *FSCN2*$^{p/p}$ neo(−) mice. The b-wave amplitudes were diminished in both. (**Q–T**) Light-adapted ERGs from 4-week-old (**Q**) *FSCN2*$^{+/g}$ neo(−) and (**R**) *FSCN2*$^{g/g}$ neo(−) mice and from 32-week-old (**S**) *FSCN2*$^{+/g}$ neo(−) and (**T**) *FSCN2*$^{g/g}$ neo(−) mice. Stimulus intensity of all recordings was 1.0 cd/m^2.

(Figs. 8K, 8L, 9C), but at 32 weeks, they were significantly smaller than those of wild-type mice ($P < 0.05$; Figs. 8N, 8O, 9C). In the homozygous *FSCN2*$^{p/p}$ neo(−) mice, the photopic b-wave amplitudes were much smaller than those of the wild-type and *FSCN2*$^{+/p}$ neo(−) mice, even at 4 weeks, and progressively deceased with increasing age (Figs. 8M, 8P, 9C). The differences in the scotopic and photopic ERGs between the p-type neo(+) and -(−) mice were not significant (data not shown).

The scotopic and photopic ERGs of *FSCN2*$^{+/g}$ neo(+) and *FSCN2*$^{g/g}$ neo(−) mice were very similar to those of the *FSCN2*$^{+/p}$ neo(−) and *FSCN2*$^{p/p}$ neo(−) mice, respectively (Figs. 8G–J, 8Q–T, 9A–C). The differences between scotopic and photopic ERGs were not significant in the g-type neo(+) and -(−) mice (data not shown).

Discussion

Our results demonstrated that the degree of photoreceptor degeneration in heterozygous mice with the exon 1-null allele and the point mutation allele increased with age. The alteration included shortening of the OS, thinning of the ONL and INL, and reduction in the number of the nuclei in the ONL and INL. The OS of *FSCN2*$^{+/p}$ and *FSCN2*$^{+/g}$ mice at 4 weeks of age were shorter than in wild-type mice of the same age, and the shortening was greater in older mice. In the TEM analyses, the OS of *FSCN2*$^{+/p}$ and *FSCN2*$^{+/g}$ mice were shorter, agreeing with the LM examination. These observations suggest that the formation of discs is delayed in the photoreceptors of *FSCN2*$^{+/p}$ and *FSCN2*$^{+/g}$ mice. The thinning of the INL in *FSCN2*$^{+/p}$, *FSCN2*$^{p/p}$, *FSCN2*$^{+/g}$, and *FSCN2*$^{g/g}$ mice followed photoreceptor degeneration. These findings suggest that the degeneration of bipolar cells in the INL was among the secondary changes.

In contrast, the length of the OS of *FSCN2*$^{p/p}$ and *FSCN2*$^{g/g}$ at 4 weeks of age was significantly shorter than that of *FSCN2*$^{+/p}$ and that of *FSCN2*$^{+/g}$ at the same age, and the OS were extremely bent in the TEM analyses. The length of the OS of *FSCN2*$^{p/p}$ and *FSCN2*$^{g/g}$ also shortened with increasing age.

The question then arises as to the mechanism causing the photoreceptor degeneration. There is a meshwork of actin filaments at the distal end of the connecting cilium.[17–20] Individual actin filaments radiate from the meshwork into the base of OS discs by passing between pairs of ciliary microtubule doublet.[21] Rhodopsin is densely packed in the membrane of the photoreceptor connecting cilia and axonemal actin in the connecting cilium, which is spatially colocalized with myosin VIIa and opsin.[22] These observations suggest that the actin filament network provides cytoskeletal support and guidance for the growing OS disks, and mediates the trafficking of membrane components including rhodopsin. In situ hybridization demonstrated hybridization signals at the inner segments of photoreceptors in wild-type mice, but no signal was observed in *FSCN2*$^{p/p}$ mice. The OS discs of *FSCN2*$^{p/p}$ and *FSCN2*$^{g/g}$ retinas were misaligned at the distal end of the connecting cilium, and this misalignment was stronger with increasing age. FSCN2 incudes actin binding and actin-bundling activity in vitro.[12] In vivo, *Drosophila* fascin (singed) is necessary for actin bundle assembly in developing bristles and in the nurse cell cytoplasm of egg chambers.[23] When *Drosophila* nurse cell cytoplasmic actin bundles are absent, the rapid phase of nurse cell cytoplasm transport is blocked, and mature eggs are only 50% the size of wild-type eggs. In severely singed mutants, the small disorganized actin filament bundles lack structural integrity and allow bristles to bend, like the OS of *FSCN2*$^{p/p}$ and *FSCN2*$^{g/g}$. Taken together, the observations in the *FSCN2*$^{p/p}$ and *FSCN2*$^{g/g}$ retinas imply that mutations of FSCN2 may hamper maintenance and/or elongation of OS disks and decrease the function of the photoreceptors.

Recent molecular genetic analyses have shown that inherited retinal degeneration has allelic and nonallelic heterogeneity and that the phenotype depends on the type of mutation. Thus, mutations of peripherin/*RDS* and *ABCA4* genes can lead to MD or RP in humans,[24–26] and an identical 1147delA mutation in the arrestin gene is the cause not only of Oguchi disease but also of autosomal recessive RP.[27–29] In our mice, the scotopic a- and b-wave amplitudes of *FSCN2*$^{+/p}$ and *FSCN2*$^{+/g}$ decreased with increasing age, corresponding to the histologic changes. The 208delG mutation in the *FSCN2* gene causes ADMD at a young age in humans, with degeneration mainly of the cones, and it also causes ADRP in humans. The photopic b-wave amplitudes of all heterozygous *FSCN2*$^{+/p}$ and *FSCN2*$^{+/g}$ mice, however, decreased much later than the decrease in the scotopic b-wave amplitudes. These observations suggest that the photoreceptor degeneration in *FSCN2* mutant mice resembles RP, but not MD, in humans. The mouse retina has significantly fewer cones than does the human retina, and there is no manifest macula as in primates. It is unclear whether these anatomic differences and/or other factors affect the phenotypes observed in *FSCN2* mutant mice. Further analysis may help to resolve this question.

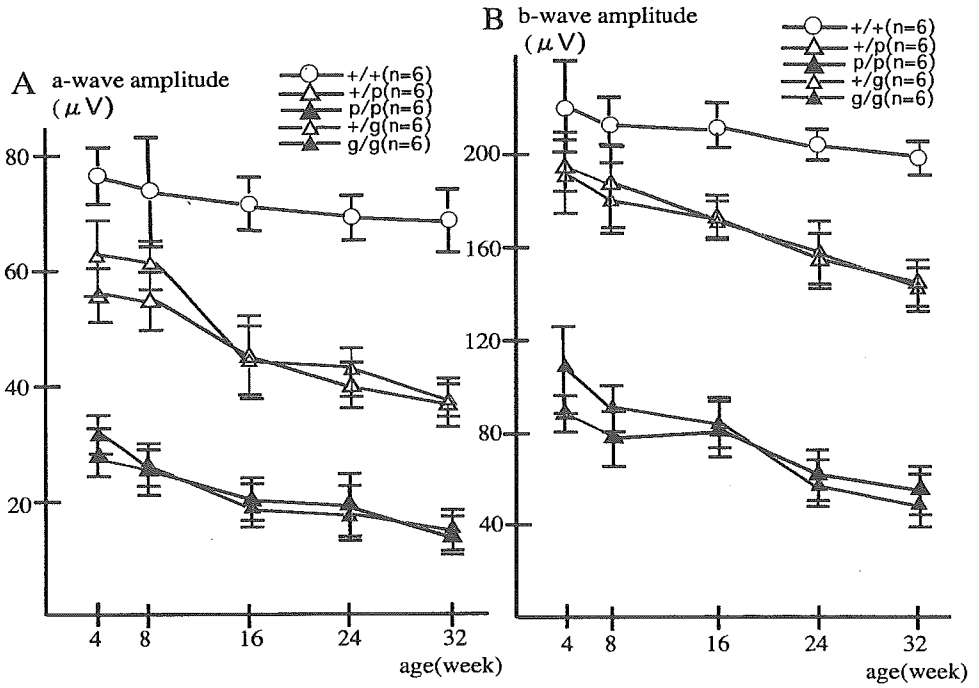

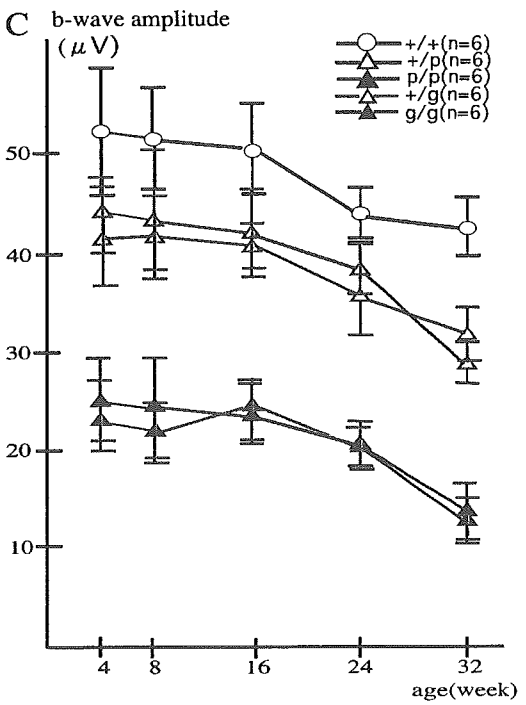

FIGURE 9. Time course of dark-adapted (A) a- and (B) b-wave amplitudes. The a- and b-wave amplitudes of scotopic ERGs were diminished in both homozygous and heterozygous mutant mice with increasing age. (C) Time course of light-adapted b-wave amplitude change. The b-wave amplitudes of photopic ERGs were decreased in both heterozygous and homozygous mutant mice. The decrease was observed later than that in scotopic ERGs. Data are the mean ± SEM. Labels for genotypes are as described in Figure 5; $n = 6$ for each genotype.

RT-PCR analyses demonstrated that mouse *FSCN2* mRNA was not transcribed in the g-type allele because the transcription was prevented by a poly(A) signal added to the 3′ end of the cDNA of GFP. Alternatively, our results showed that all the *FSCN2* mRNA was degraded in both $FSCN2^{p/p}$ neo(+) and -(−) mice. A nonsense-mediated decay mechanism may degrade the mRNA with an abnormal stop codon (codon 140).[30] The p-type mutant mice with a single-base deletion were phenotypically similar to the g-type mutant mice that did not have exon 1 of the *FSCN2* gene. These results suggest that the mutant *FSCN2* gene (208delG mutation) did not produce FSCN2 protein, and therefore haploinsufficiency of the FSCN2 protein may cause RP in human heterozygotes.

In conclusion, we produced *FSCN2* mutant mice by gene targeting techniques. The $FSCN2^{+/p}$ and $FSCN2^{+/g}$ mice had decreased rod function that worsened with increasing age and was followed by reduction of cone function. In patients with RP, rod photoreceptor abnormalities precede the onset of cone abnormalities typically.[31] Therefore, the phenotypes of our mice may resemble RP, not MD, in human heterozygotes. Our results suggest that haploinsufficiency of *FSCN2* may alter maintenance and/or elongation of OS disks and induce photoreceptor degeneration. However, more detailed analyses of photoreceptor morphogenesis in these mouse models are needed to understand the mechanism of photoreceptor degeneration. We suggest that these mice are good models to study

the mechanisms for the changes found in human ADRP caused by mutations of the *FSCN2* gene.

References

1. Pagon RA. Retinitis pigmentosa. *Surv Ophthalmol.* 1988;33:137-177.
2. Berson EL, Sandberg MA, Rosner B, Birch DG, Hanson AH. Natural courses of retinitis pigmentosa over a three-year interval. *Am J Ophthalmol.* 1985;99:240-251.
3. Ali RR, Sarra GM, Stephenes C, et al. Restoration of photoreceptor ultrastructure and function in retinal degeneration slow mice by gene therapy. *Nat Genet.* 2000;25:306-310.
4. Chow AY, Chow VY, Packo KH, et al. The artificial silicon retina microchip for the treatment of vision loss from retinitis pigmentosa. *Arch Ophthalmol.* 2004;122:460-469.
5. RetNet. Cloned and/or mapped genes causing retinal diseases. Available at: http://www.sph.uth.tmc.edu./RetNet/disease.htm. Accessed May 27, 2004.
6. Iannaccone A. Genotype-phenotype correlations and differential diagnosis in autosomal dominant macular diseases. *Doc Ophthalmol.* 2001;102:197-236.
7. Mac Donald IM, Hebert M, Yau RJ, et al. Effect of docosahexaenoic acid supplementation on retinal function in a patient with autosomal dominant Stargardt-like macular dystrophy. *Br J Ophthalmol.* 2004;88:305-306.
8. Holz FG, Haimovici R, Wagner DG, Bird AC. Recurrent choroidal neovascularization after laser photocoagulation in Sorsby's fundus dystrophy. *Retina.* 1994;14:329-334.
9. Wada Y, Abe T, Takeshita T, et al. Mutation of human retinal ascin gene (FSCN2) causes autosomal dominant retinitis pigmentosa. *Invest Ophthalmol Vis Sci.* 2001;42:2395-2400.
10. Wada Y, Abe T, Itabashi T, et al. Autosomal dominant macular degeneration associated with 208delG in FSCN2 gene. *Arch Ophthalmol.* 2003;121:1613-1620.
11. Tubb BE, Bardien-Kruger S, Kashork CD, et al. Characterization of human retinal fascin gene (FSCN2) at 17q25: close physical linkage of fascin and cytoplasmic actin genes. *Genomics.* 2000;65:146-156.
12. Saishin Y, Ihikawa R, Ugawa S, et al. Retinal fascin: functional nature, subcellular distribution, and chromosomal localization. *Invest Ophthalmol Vis Sci.* 2000;41:2087-2095.
13. Saishin Y, Shimada S, Morimura H, et al. Isolation of a cDNA encoding a photoreceptor cell-specific actin-bundling protein: retinal fascin. *FEBS Lett.* 1997;414:381-386.
14. Quon KC, Berns A. Haplo-insufficiency?—let me count the ways. *Gen Dev.* 2001;15:2917-2921.
15. Minowa O, Ikeda K, Sugitani Y, et al. Altered cochlear fibrocytes in a mouse model of DFN3 nonsyndromic deafness. *Science.* 1999;285:1408-1411.
16. Obin M, Pike A, Halbleib M, et al. Calorie restriction modulates age-dependent changes in the retinas of Brown Norway rats. *Mech Ageing Dev.* 2000;114:133-147.
17. Chaitin MH, Schneider BG, Hall M, Papermaster DS. Actin in the photoreceptor connecting cilium: immunological localization to the site of outer segment disk formation. *J Cell Biol.* 1984;99:239-247.
18. Chaitin MH, Bok D. Immunoferritin localization of actin in retinal photoreceptors. *Invest Ophthalmol Vis Sci.* 1986;27:1764-1767.
19. Chaitin MH, Carlsen RB, Samara GJ. Immunogold localization of actin in developing photoreceptor cilia of normal and *rds* mutant mice. *Exp Eye Res.* 1988;47:437-446.
20. Steinberg RH, Fisher SK, Anderson DH. Disc morphogenesis in vertebrate photoreceptors. *J Comp Neurol.* 1980;190:501-508.
21. Chaitin MH, Burnside B. Actin filament polarity at the site of rod outer segment disk morphogenesis. *Invest Ophthalmol Vis Sci.* 1989;30:2461-2469.
22. Wolfrum U, Schmitt A. Rhodopsin transport in the membrane of the connecting cilium of mammalian photoreceptor cells. *Cell Motil Cytoskeleton.* 2000;46:95-107.
23. Cant K, Knowles BA, Mooseker MS, Cooley L. *Drosophila* singed, fascin homolog, required for actin bundle formation during oogenesis and bristle extension. *J Cell Biol.* 1994;125:369-380.
24. Paloma E, Coco R, Martinez-Mir A, et al. Analysis of ABCA4 in mixed Spanish families segregating different retinal dystrophies. *Hum Mutat.* 2002;20:476.
25. Fukui T, Yamamoto S, Nakano K, et al. ABCA4 gene mutations in Japanese patients with Stargardt disease and retinitis pigmentosa. *Invest Ophthalmol Vis Sci.* 2002;43:2819-2824.
26. Shroyer NF, Lewis RA, Yatsenko AN, Lupski JR. Null missense ABCR (ABCA4) mutations in a family with Stargardt disease and retinitis pigmentosa. *Invest Ophthalmol Vis Sci.* 2001;42:2757-2761.
27. Nakazawa M, Wada Y, Tamai M. Arrestin gene mutations in autosomal recessive retinitis pigmentosa. *Arch Ophthalmol.* 1998;116:498-501.
28. Wada Y, Nakazawa M, Tamai M. A patient with progressive retinal degeneration associated with homozygous 1147delA mutation in the arrestin gene. In: La Vail MM, Anderson RE, Hollyfield JG, eds. *Retinal Degenerative Disease.* New York: Plenum Press; 1997:319-322.
29. Nakazawa M, Wada Y, Fuchs S, Gal A, Tamai M. Oguchi disease: phenotypic characteristic of patients with the frequent 1147delA mutation in the arrestin gene. *Retina.* 1997;17:17-22.
30. Zhang J, Maquat LE. Evidence that the decay of nucleus-associated nonsense mRNA for human triosephosphate isomerase involves nonsense codon recognition after splicing. *RNA.* 1996;2:235-243.
31. Heckenlively JR. Clinical findings in retinitis pigmentosa. In: Heckenlively JR, ed. *Retinitis Pigmentosa.* Philadelphia: JB Lippincott; 1988:68-89.

8. ゼブラフィッシュ変異体をモデルとして用いた視細胞死の原因の検討

辻川元一、田野保雄
（大阪大）

研究要旨　ゼブラフィッシュのENU誘導変異体oval(ovl)は視細胞の変性、腎臓の嚢胞、体軸の湾曲を三主徴とする変異体で、腎臓の奇形と視細胞の変性よりヒトのBBS症候群のモデルと考えられている。ポジショナルクローニングの結果、ovlはゼブラフィッシュのIFT88ホモローグ(polaris)をコードしていた。IFTは繊毛における物質の輸送を担う蛋白群であり、これを欠くことにより、ovlでは感覚器受容体における繊毛が早期に喪失し、その後、感覚器受容体自体がアポトーシスを引き起こし、死滅した。視細胞においては繊毛の欠如により外節は分化せず、受精後3日目より視細胞死が観察された。外節の欠如によりロドプシンは細胞膜全体に異所性集積し、この異所性集積と光による活性化が視細胞死の進行に強く関与する事が示された。

A．研究目的

ゼブラフィッシュ視細胞変異体を用い、その責任遺伝子の単離とその機能解析を行い、色素変性等の視細胞死のメカニズムの一端を明らかにする。

B．研究方法

ゼブラフィッシュのENU誘発ゼブラフィッシュ変異体oval(ovl)は視細胞の変性、腎臓の嚢胞、体軸の湾曲を三主徴とする変異体で、腎臓の奇形と視細胞の変性よりヒトのBBS症候群のモデルと考えられている。我々はこのovlを対象とし、その責任遺伝子の同定をポジショナルクローニングを用いて行った。また、その変異体の表現系解析を免疫組織科学等を用いて遂行した。また、モルフォリノ等を用いた遺伝子発現調整を用いて、責任遺伝子の機能を明らかにすると共に、視細胞死を引き起こす原因についても検討した。

C．研究結果

連鎖解析の結果ovlはゼブラフィッシュ第9番染色体のセントロメア近傍領域にマップされた。この位置にはIFT88 (polaris)のホモローグをコードするESTがマップされており、この全長を単離し、塩基配列解析を行ったところこの遺伝子のエクソン11にナンセンス変異が検出された（L260X)。この変異により少なくとも9つあるTPRリピートの2つ目以降は翻訳されず、他の結果も含め、この変異はNull変異考えられた。我々が正しいローカスをクローニングしていることを確認するため、正常胚に抗IFT88モルフォリノをイジェクションしその表現系の変化を見たところ、体軸の変異、鼻の

繊毛の喪失といったovlの表現系をコピーしていた。逆にovl変異体にIFT88mRNAをインジェクションすると正常の表現系を回復した。これらの結果より、我々はovlはゼブラフィッシュIFT88をコードしていると結論づけた。

ovlでは視細胞を含む感覚器受容細胞は受精後３−５日目までに繊毛の喪失が認められた。この繊毛の喪失は視細胞においては外節の発生に影響し、ovlにおいては視細胞外節の分化がみとめられなかった。しかしながら、電子顕微鏡的検索においてはovlの視細胞は外節の欠如以外に大きな構造学的異常を認めなかった。内節、細胞体、シナプス結合部はどれも野生型と区別しがたかったが、唯一、細胞側壁において重層化した膜様構造物を認め、その構造より、異所性の外節ではないかと考えられた。

このように構造学的には比較的正常に近いovl視細胞であるが、受精後３日目よりアポトーシスを引き起こし、死滅していった。このアポトーシスは他の感覚器受容体においても繊毛の喪失後に認められた。したがって、IFT88は繊毛の維持と感覚器細胞の生存に不可欠であると結論された。

ovl視細胞は繊毛が比較的早期に喪失するため、外節が分化しない。このため、外節に輸送されるべき視物質、たとえば、ロドプシンは外節にではなく、細胞膜全体に異所性に蓄積していた。ovl視細胞において、この異所性ロドプシンの発現を抗ロドプシンモルフォリノを用いて抑制した場合、対象に比べ、受精後4.5日目においてRODの５０％以上多く生存していた。これに対して、抗ロドプシンモルフォリノの影響を受けない錐体受容体の数は両者の間に差は認めなかった。少なくとも、異所性ロドプシンの発現が視細胞死を促進していることが示された。

さらに、この視細胞死は光感受性を示した。明条件下（これ自体では野生型視細胞に細胞死を引き起こさない。）においてovl視細胞はより早く重篤な変性を示すのに対し、暗条件下では視細胞死は有意に抑制された。この光刺激による視細胞死の誘導はわずか３６時間の光刺激でも誘導され、光刺激による異所性ロドプシンの活性化は視細胞死を強く促進する事が示唆された。

D．考案

網膜色素変性は遺伝子座多型生がきわめて高い疾患郡である。これに対して、フォトトランスダクション経路の解明とヒトゲノム情報の開示をうけ、多くの責任遺伝子が単離されたが、それらの機能解析は進んでいるとは言えず、視細胞死にいたるメカニズムのほとんどは不明のままである。視細胞研究の問題点の一つは良いvitroのモデルが存在しない点にあり、研究は遺伝子改変マウスを用いたものが中心となるであろうが、その作成や維持にはある程度の労力を必要とし、現在の大学一般の現状とはなじみにくい。この問題に対する解決法の一つとして、今回我々はゼブラフィッシュ変異体を用いて、視細胞死のメカニズムの一端を解明した。このモデル動物は、多産、体外受精、早い世代期間といった優れた特徴を持っており、脊椎動物における疾患モデル動物として、今後有用であると考えられた。

我々の変異体ovlは結果的には繊毛のたんぱく質である。IFT88ホモローグをコード

しており、その結果、外節の発生が認められなかった。近年、この繊毛における遺伝子解析と機能は基礎生物学でも注目を集めている分野であり、事実、明らかとなってきたBBS症候群の責任遺伝子群は繊毛のたんぱく質の機能解析の延長上で単離されてきている。我々の機能解析により、繊毛の輸送を担う蛋白複合体IFTは視細胞を含めた感覚器細胞の維持に必要であることが示された。

さらに、この変異体で認められた、異所性ロドプシンの蓄積は網膜色素変性症の患者、および、モデル動物において認められる病態である(Sung et al; Gao et al; Nishimura et al.)。それのみでなく、網膜剥離(Lewis et al)、加齢黄斑変性(Johnson et al.)等の病態でも認められ、視細胞死との関連が示唆されていた。今回、ゼブラフィッシュを用いた遺伝子発現制御（ロドプシン発現抑制）により、はじめて、直接的にこの関連が証明された。さらに、我々は、この異所性ロドプシンが光子により活性化されることが視細胞死を促進することを示した。このことは、フォトトランスダクションがオンに細胞死のシグナル伝達に重要であることを示唆している。網膜色素変性においてはPRGR遺伝子産物がやはり繊毛における物質の輸送への関与が示唆されており、我々のovlはこの病態の端的な状態を再現していることが期待される。今後はこのシグナルの詳細の解析が課題となる。

我々は他のゼブラフィッシュ視細胞変異体(mok)についてもその責任遺伝子を同定し、解析をほぼ終了している（現在投稿中)。この変異体においては視物質の輸送は正常であり、ovlとは異なったメカニズムで視細胞を引き起こしていると考えられ興味深い。

E. 結論

ゼブラフィッシュ変異体ovlは繊毛の輸送蛋白IFT88がその責任遺伝子であった。IFT88は感覚器受容体の維持に不可欠であり、視細胞においてはロドプシンの局在異常をひきおこし、この病態は視細胞死を促進する要因である。

F. 健康危機情報

なし

G. 研究発表

1. 論文発表

1. Tsujikawa M, Malicki J: Neuron42: 703-716, 2004.
2. Tsujikawa M, Malicki J: Int J Dev Biol. 48: 925-934, 2004.

2. 学会発表

1. Tsujikawa M, Doerre G, Malicki J. Genetic analysis of photoreceptor development. 5th International conference on zebrafish development & genetics. (Medison)
2. Tsujikawa M., Doerre G,. Malicki J. Characterization of key regulator of photoreceptor development, mikre oko. 3rd European Conference on zebrafish and medaka genetics and development (Paris)
3. Pujic Z., Tsujikawa M., Thisse B., Thisse C. Reverse genetic analysis of neuro genesis in the retina. 3rd European Conference on zebrafish

and medaka genetics and development (Paris)

4. Tsujikawa M, Malicki J. Ovl is essential for differentiation and survival of vertebrate sensory neurons (Florida)
5. Tsujikawa M, Malicki J. Ovl is essential for differentiation and survival of vertebrate sensory neurons 6th International conference on zebrafish development & genetics (Wisconsin)
6. Tsujikawa M, Malicki J. mikre oko, a regulator of photoreceptor differentiation. 6th International conference on zebrafish development & genetics (Wisconsin)

H. 知的財産権の出願・登録状況

1. 特許取得

なし

2. 実用新案登録

なし

3. その他

なし

I. 参考文献

1. Sung et al: J Neurosci. 14: 5818, 1994.
2. Gao et al: PNAS. 99: 5698 , 2002.
3. Nishimura et al: PNAS. 101: 16588, 2004.
4. Lewis et al: IOVS .43: 2412, 2002.
5. Johnson et al: IOVS .44: 4481, 2003.